

# Synergetic hydrogen-bond network of functionalized graphene and cations for enhanced atmospheric water capture

Xiaojun Ren <sup>1</sup>, Xiao Sui <sup>2</sup>, Llewellyn Owens <sup>3</sup>, Dali Ji <sup>1</sup>, Xinyue Wen <sup>1</sup>, Yuta Nishina <sup>4</sup>, Kamal K. Pant <sup>5</sup>, Vanesa Quintano <sup>1,6</sup>, Daria V. Andreeva <sup>7,8</sup>, Kostya S. Novoselov <sup>7,8</sup>, Amir Karton <sup>9\*</sup>, Tobias Foller <sup>1\*</sup>, Rakesh Joshi <sup>1\*</sup>

<sup>1</sup>School of Materials Science and Engineering, University of New South Wales Sydney, NSW 2052, Australia

<sup>2</sup>Harbin Institute of Technology (Weihai), School of Marine Science and Technology, Weihai 264209, China

<sup>3</sup>Vesi Water Pty Ltd, NSW 2340, Australia

<sup>4</sup>Graduate School of Natural Science and Technology, Okayama University, Kita-ku, Okayama, Japan

<sup>5</sup>Department of Chemical Engineering, Indian Institute of Technology Roorkee, Roorkee 247667, India

<sup>6</sup>Catalan Institute of Nanoscience and Nanotechnology (ICN2), CSIC and BIST, Campus UAB, Bellaterra, 08193 Barcelona, Spain

<sup>7</sup>Institute for Functional Intelligent Materials, National University of Singapore, Singapore, 117575 Singapore

<sup>8</sup>Department of Materials Science and Engineering, National University of Singapore, 117575, Singapore

<sup>9</sup>School of Science and Technology, University of New England, Armidale, NSW 2351, Australia

## Abstract

Water molecules at the solid-liquid interface display intricate behaviours sensitive to small changes. The presence of different interfacial components, such as cations or functional groups, shape the physical and chemical properties of the hydrogen bond network. Understanding such interfacial hydrogen-bond networks is essential for a large range of applications and scientific questions. To probe the interfacial hydrogen-bond network, atmospheric water capture is a powerful tool. Here, we experimentally observe that a calcium ion on a calcium-intercalated graphene oxide aerogel (Ca-GOA) surface captures 2.7 times more water molecules than in its freestanding state. From density functional theory (DFT) calculations, we uncover the synergistically enhanced hydrogen-bond network of the calcium ion-epoxide complex due to significantly larger polarizations and hydrogen bond enthalpies. This study reveals valuable insights into the interfacial water hydrogen-bond network on functionalized carbon-cation complexed surfaces and potential pathways for future atmospheric water generation technologies.

## Introduction

Under humid or aqueous conditions, interfacial water molecules are ubiquitous in nature and technology. The solid-liquid interface is vital in countless physical, chemical, or biological processes and applications<sup>1-4</sup>. One important factor to understand the structural properties of interfacial water is the hydrogen bond network at the interface, which is notoriously difficult to probe<sup>1,3</sup>. Recent studies revealed an exciting way to study the interfacial hydrogen network within MOFs<sup>5,6</sup> and graphene capillaries<sup>7</sup> via atmospheric water capture (AWC)<sup>8-10</sup>. It is now appealing to further broaden the use of this methodology. Firstly, extend AWC beyond the specific case of MOFs or the perfect graphene plane as the solid adsorbent. These materials consider special cases which have few technological and natural analogues. In contrast, functionalised carbon in humid or aqueous environments are ubiquitous and thus relevant in many systems. For example, the hydrophilic groups in lipid bilayers or DNA strands<sup>11,12</sup> as well as in hydrophilic polymer membranes<sup>13,14</sup>, graphene oxide-based membranes<sup>15-19</sup> or single atom catalysts<sup>20,21</sup> all obtain carbon-oxygen interfaces with water.

All these examples exist in aqueous environments that contain cations. However, there is lack of studies looking at the carbon-oxygen interface with water in the presence of cations despite its enormous fundamental and technological relevance. Hence, conceiving an AWC study that can investigate the interfacial hydrogen network in functionalised carbon under the presence of cations is highly desirable. Here, we solve this issue by utilising functionalised graphene (graphene oxide) as a representative of functionalised carbon. Graphene oxide (GO) can be readily intercalated with cations which allows probing the interfacial hydrogen network of functionalised carbon under the presence of cations via AWC.

Graphene oxide is composed of a graphene plane along with various oxygen functionalities<sup>22-26</sup>. The presence of functionalised areas gives rise to stable dipole sites and development of a hydrogen bond network with water molecules<sup>15,16</sup>. Water transport via GO based materials has been widely studied in experiments and simulations to better understand its surface interaction with water molecules<sup>27-34</sup>. Yet, direct experimental evidence is still limited for progressive understanding of the hydrogen-bond network on the GO surface. The most recent water transport study highlighted that intercalated cation on GO surface causes controllable friction with water molecules via hydrogen bondings<sup>16</sup>. The observations suggest that intercalated cations may enrich the hydrogen bond network of water molecules on GO

surface. With that, cation intercalated GO offers a unique platform to investigate the hydrogen network of functionalized carbon in a cationic aqueous solution, which is highly relevant in many fields.

In this study, we use AWC to reveal that the interaction of cation and oxygen functionalised carbon induces synergistic enhancement of the interfacial hydrogen bond network in aqueous environment. Here, we choose calcium ions due to its outstanding atmospheric water capture ability<sup>35</sup>. This allows us to sensitively detect changes in the hydrogen-bond network in GO due to the presence of the cations. We synthesized calcium-intercalated GO (Ca-GO) in aerogel form and measured the atmospheric water capture capability of the as prepared material. Surprisingly, we experimentally observed that calcium-intercalated GO aerogel (Ca-GOA) presents significantly different water uptake ability than original GO and CaCl<sub>2</sub>. Via further in-depth experimental analysis and computational simulations, this study reveals an enhanced water hydrogen-bond network which is governed by a so far undiscovered synergistic enhancement between oxygen functionalities of GO and hydrated cations. We find that this strong hydrogen-bond network gives rise to new AWC technology using GO-based materials.

## Results

Based on our aim to investigate the functionalised carbon-cation interfacial water hydrogen-bond network, we prepared GO/CaCl<sub>2</sub> aerogel via solution intercalation method<sup>36</sup>. The synthesis procedure is shown in Fig.S1a and described in detail in the methods section. The as synthesized samples are marked as GOA for graphene oxide aerogel and Ca-GOA for Ca<sup>2+</sup> intercalated GO aerogel respectively. Exemplary images of GOA and Ca-GOA are displayed in Fig. S1b-d.

We characterised the structure and chemical properties of the samples before and after intercalation. Scanning electron microscopy (SEM) with energy dispersive spectroscopy (EDS) images are shown in Fig. 1a-c and Fig. S2b-c (see supplementary note 2), illustrating the sample morphology. The synthesized Ca-GOA samples display a porous structure similar to the GOA sample with typical wrinkled large surface area. X-ray photoelectron spectrometry (XPS) reveals that the carbon to oxygen ratio (C/O) of GO remains constant at ~2 before and after intercalation (Fig.1d). C1s XPS spectra curves further suggest that Ca-GOA (Fig.1f) have similar carbon-carbon and carbon-oxygen bonds composition compared to GO samples (see

Fig.S3a-d in supplementary note 3). The XPS survey and atomic percentage of each element for both GO and Ca-GOA are shown in Fig. 1f. Around 5.1% of calcium atoms are detected on the Ca-GOA surface, while in the original GO, no calcium was detected. This confirms the successful intercalation of Ca-ions into the Ca-GOA samples. It is noted that a small number of chlorine and sulfur atoms are also detected on Ca-GOA however are not the main concern in this study.

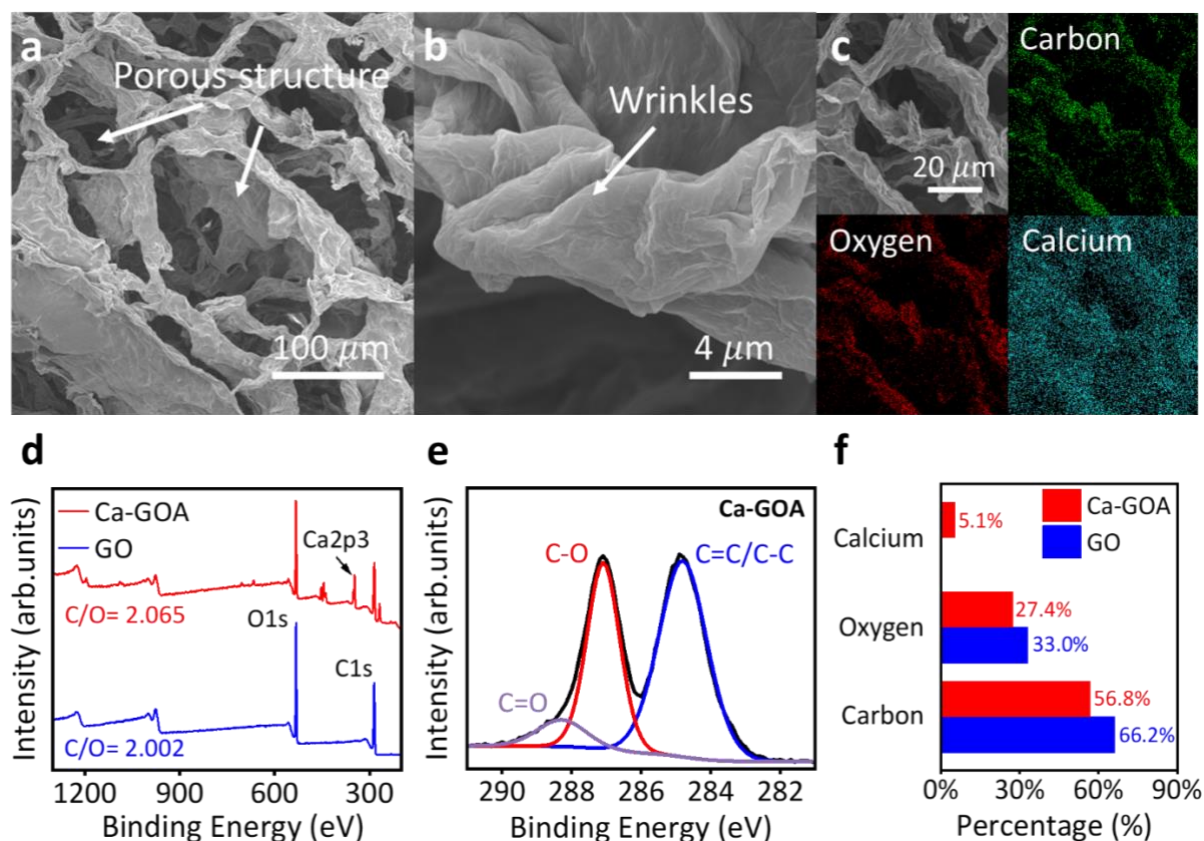


**Fig.1 Characterization of Ca-GOA.** **a** Scanning electron microscopy (SEM) image of the overall structure of Ca-GOA. **b** SEM image of Ca-GOA showing typical wrinkles. **c** SEM image of Ca-GOA with energy dispersive spectroscopy (EDS) showing elemental images of carbon, oxygen, and calcium. **d** X-ray photoelectron spectrometry (XPS) survey of GO and Ca-GOA showing C1s, O1s and Ca2p3 peak with carbon/oxygen (C/O) ratio. **e** XPS spectra (black curve) showing C1s peak of Ca-GOA sample with peak fitting of C=C/C-C bond at  $\sim 284.5$  eV, C-O bond (red curve) at  $\sim 286$  eV and C=O bond (purple curve) at  $\sim 288$  eV. **f** Atomic percentage of elemental composition including calcium, oxygen and carbon of GO and Ca-GOA samples.

To investigate the hydrogen-bond network in the Ca-GOA, we performed AWC measurements as described in the methods section and compared the results to literature values from our own studies and others<sup>35,37</sup>. Fig.2a-c show the recorded and reported adsorption isotherms. The water uptake ( $m/m_0$ ) of Ca-GOA was recorded with varying relative humidity (RH%) at

constant room temperature (298K). The relative humidity is then converted into the partial pressure of water vapor to visualise the isotherm. The results show that AWC ability of Ca-GOA samples is significantly improved to up to 2.1 g/g from pure GO samples (GOM) with 0.5 g/g, which indicates the enriched hydrogen network on Ca-GOA surface. It should be noted that the referred GO adsorption curve was measured for GO membranes (GOM) and not in the form of aerogel. However, we ruled out the influence of materials morphology for AWC by showing that GOM and pure GOA have similar AWC ability (supplementary note 3).

Further analysis of the isotherms allows us to get a deeper understanding of interfacial water molecules during the AWC. All three different materials,  $\text{CaCl}_2$ <sup>35</sup>, GOM<sup>37</sup> and our measured data of Ca-GOA, fit well under the BET model<sup>38,39</sup>. However, the fitted BET equations are notably different from each (see supplementary note 4 for fitting details). The degree of the polynomial function of the BET equation, represents the number of adsorbed water molecule layers ( $n$ ) on the surface of the material<sup>35,39,40</sup>. Here,  $n=7$  for  $\text{CaCl}_2$ ,  $n=4$  for GOM and  $n=6$  for Ca-GOA. Hence, the intercalation of Ca into Ca-GOA results in a stronger hydrogen network on surface compared to pure GO. In other words, the intercalation of cation enhances the interfacial water hydrogen network at the oxidized carbon surface, however the mechanism of such enhancement is still unclear.

Based on the BET model fitting analysis, we established that the Ca-intercalation offers strong adsorption sites for water molecules on the Ca-GOA surface. If that is the case, the adsorption isotherm should follow the Freundlich model, as it represents a heterogeneous surface adsorption process<sup>41</sup>. In particular, Freundlich model describes a material with special adsorbing sites which are heterogeneously distributed on the adsorbent surface<sup>42-44</sup>. In this case, the Ca atoms are the strong water-attracting adsorbing sites, well-dispersed on the GO plane, allowing coverage of the whole surface with several layers of water molecules<sup>45</sup>. As shown in Fig. 2d-f, the water adsorption isotherm of Ca-GOA can be fitted in high agreement with the typical Freundlich isotherm model, while being less in agreement with GO and  $\text{CaCl}_2$ . The detailed information for Freundlich model fitting is shown in supplementary note 5.

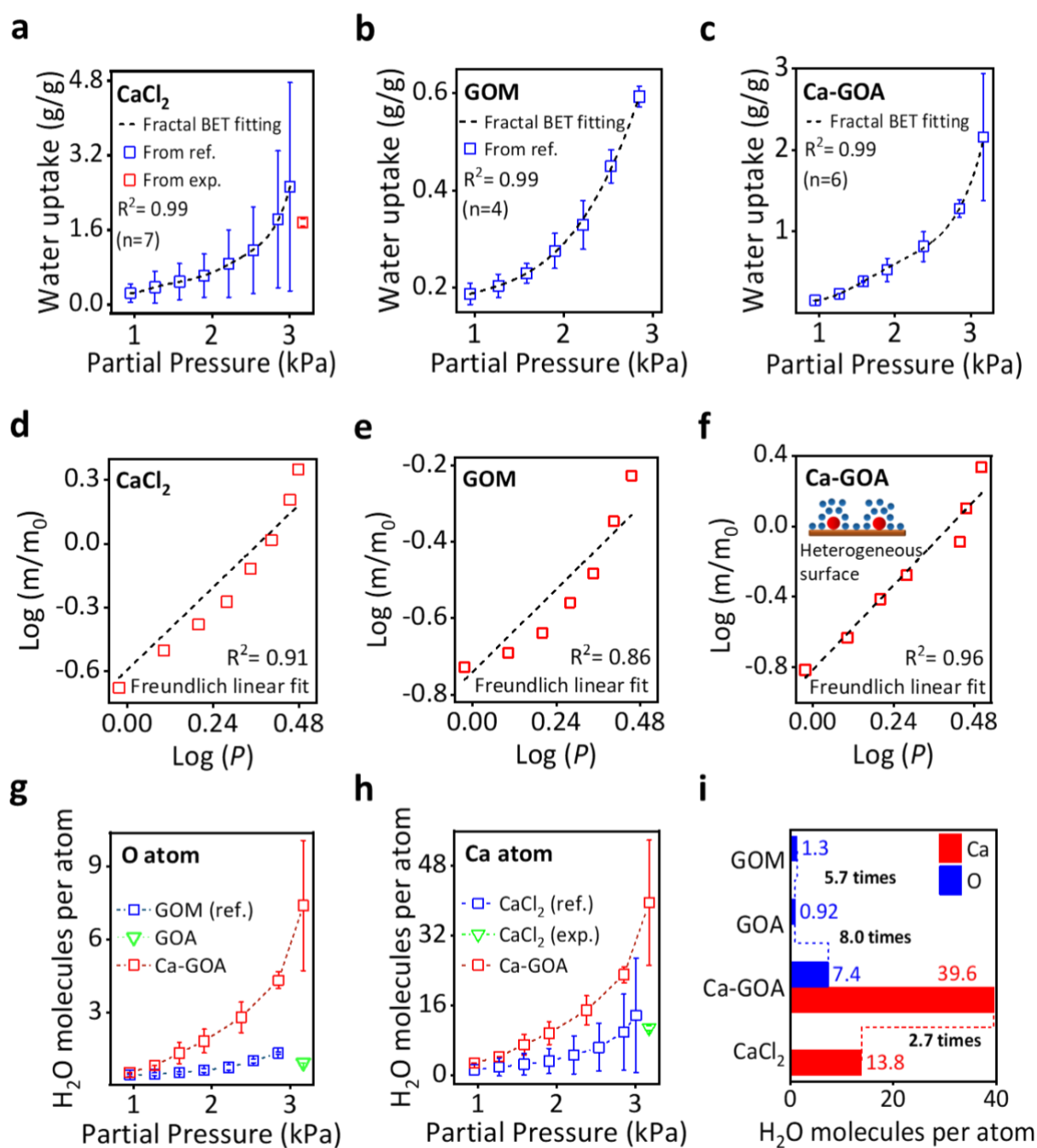


**Fig.2 Adsorption isotherm of CaCl<sub>2</sub>, GOM and Ca-GOA.** **a-c** Water uptake of CaCl<sub>2</sub> (**a**), GOM (**b**) and Ca-GOA (**c**) under different ambient water partial pressure (kPa). The error bar indicates the standard deviation. Black dashed lines illustrate the fractal BET fitting of CaCl<sub>2</sub>, GOM, and Ca-GOA. **d-f** Freundlich linear fitting (black dashed line) of CaCl<sub>2</sub> (**d**), GOM (**e**) and Ca-GOA (**f**). The inset diagram in (**f**) indicates the heterogeneous adsorption behaviours of Freundlich model.  $R^2$  represents the coefficient of determination of the fitting. **g-h** Comparison of estimated water molecules per oxygen (**g**) and calcium atom (**h**) between GOM, GOA and Ca-GOA under different ambient water partial pressure (kPa). **i** Estimation of the highest number of water molecules per oxygen/calcium atom in CaCl<sub>2</sub>, Ca-GOA, GOA and GOM based on the experimental observation of water uptake.

The trend of water molecules per oxygen and calcium atom of GOM, GOA, Ca-GOA and CaCl<sub>2</sub>



versus the water partial pressure are shown in Fig. 2g-h. The uptake of water molecules per oxygen atom on Ca-GOA is up to 8 times higher than that of GOM and GOA at all ambient environments. Surprisingly, the water uptake per calcium ion, is up to 2.7 times higher in Ca-GOA compared to CaCl<sub>2</sub> at the highest water partial pressure (Fig.2i).

Here, we can conclude that the water uptake per calcium and oxygen atom in Ca-GOA is much higher than in the individual materials, CaCl<sub>2</sub> and GOA/GOM. Keeping in mind that the Ca-sites were identified as the main contributor to the water uptake in Ca-GOA, it is striking to see that the water uptake per calcium is 2.7 times higher in the Ca-GOA compared to CaCl<sub>2</sub>. This strongly suggests that this enhancement is linked to an interplay between the functional groups of GO and the intercalated cations to form a synergistically enhanced hydrogen-bond network. To investigate this hypothesis, we further performed density functional theory (DFT) calculations.

We examine the hydrogen bond properties between oxygen functionalities and water molecules with and without the existence of calcium ions using DFT calculation. We select a graphene plane with a bare epoxide group as a simplified model of a GO nanoflake surface as shown in Fig. 3a. Epoxide and hydroxide groups are typical oxygen functionalities on the GO basal plane and have been experimentally confirmed to have a strong hydrogen bonding interaction with water molecules<sup>32,46</sup>. The DFT calculations were performed at the PBE0-D3BJ/def2-QZVPP level of theory<sup>47-49</sup>. Fig. 3b-c indicates the process of the epoxide hydrogen bonded to one and two water molecules. We obtain hydrogen bond distances and energies typical of moderate hydrogen bonds<sup>50-52</sup>. Namely, both water molecules hydrogen bonded to the epoxide group with a distance range of 1.96–1.99 Å and enthalpy of –14.8 kJ/mol and –13.4 kJ/mol for the first and second water molecule, respectively. However, when the hydrated calcium cation is bound to the epoxide group, the hydrogen bonding network presents significantly different properties. We note that when the epoxy oxygen is coordinated to the Ca cation, the oxygen is bound to the GO surface via one C–O bond, as illustrated in Fig. 3d-e. We note that the bonding situation in Fig. 3d-e also represents the bonding of a hydrated Ca cation to a C–O functional group on the GO surface<sup>53</sup>. Hereinafter, the oxygen connected to the GO surface with a single C–O bond will be referred to as the GO oxygen, rather than the epoxy oxygen.

With the presence of calcium cation, our calculations suggest that the GO oxygen is

coordinate to the hydrated calcium cation. This dramatically enhances the hydrogen-bond network surrounding GO oxygen. Fig. 3d presents a scenario when one water molecule is hydrogen bonded to both the GO oxygen and the hydrated calcium ion. Compared with the system in Fig. 3c, this water molecule is now hydrogen bonded via three hydrogen bonds, one with the GO oxygen and two with the hydrating water molecules around the calcium ion. As shown in Fig. 3d, the hydrogen bond formed with the GO oxygen (1.546 Å) is significantly shorter than the hydrogen bonds formed with the water molecules hydrating the calcium cation (1.699 and 1.725 Å). Furthermore, this hydrogen bond is also significantly shorter than that formed between the water molecule and bare epoxide group presented in Fig. 3b. Similarly, in Fig. 3e, we further show the scenario when the GO oxygen is hydrogen bonded to a second water molecule. The calculation shows that the length of the hydrogen bond between the GO oxygen and the second water molecule is also largely shortened, from 1.982 Å (Fig. 3c) to 1.689 Å (Fig. 3e).

From the hydrogen bond enthalpy point of view, our calculations show that the hydrogen bonding between the GO oxygen and water molecules are highly reinforced by the hydrated calcium ion. In the scenario of the bare epoxide group on the GO surface, the hydrogen bond enthalpy between the oxygen and water molecules is around  $-14$  kJ/mol, as mentioned above. However, in the presence of the hydrated calcium ion, the hydrogen bond enthalpy between the GO and water molecules in the system shown in Fig. 3d increases to as much  $-66.7$  kJ/mol and in Fig. 3e comes to  $-52.9$  kJ/mol. Thus, the H-bond enthalpy in the presence of the hydrated calcium ion is about 3–4 times higher than that of a bare system. Both the increased hydrogen bond enthalpy and shorter hydrogen bond lengths are attributed to both the larger hydrogen bond network and stronger hydrogen bonding acceptor strength of the calcium ion decorated GO oxygen.

We further investigate the hydrogen bonding acceptor properties of the GO oxygen based on the atomic polar tensor (APT) charges<sup>54,55</sup>. The results are shown in Table 1. We obtain the following APT charges of the epoxide oxygen,  $-0.40 e$ ,  $-0.47 e$ , and  $-0.51 e$  in the system shown in Fig. 3a-c, respectively. As expected, the negative charge on the oxygen increases with the number of hydrogen bonds it is involved in. The charge on the hydrogen and oxygen atoms of the water molecules remains relatively constant for systems 3b and 3c. Namely, they range between  $+0.23 e$  and  $+0.27 e$  for the hydrogen and between  $-0.45 e$  and  $-0.49 e$  for the



oxygen. Coordination of the hydrated calcium cation to the GO oxygen results in a dramatic change in the oxygen charge. In particular, the coordination of the hydrated calcium cation increases the negative charge on the GO oxygen from  $-0.40 e$  to as much as  $-0.86 e$ . This significant increase in negative charge on the GO oxygen makes it a much stronger hydrogen bond acceptor. Accordingly, the H-bond distance with the water molecule is shortened from  $1.965 \text{ \AA}$  (Fig. 3b) to  $1.546 \text{ \AA}$  (Fig. 3d). We note that the later hydrogen bond distance represents an exceptionally short hydrogen bond for a HOH...O system (i.e., a water molecule coordinated to an oxygen atom)<sup>50,51</sup>. It also reveals that coordination of calcium ion to the GO oxygen alters the atomic charges on the hydrogen and oxygen of the hydrogen-bonded water molecules. For example, for the systems depicted in Fig. 3b and 3d, the positive charge on the hydrogen increases from  $+0.27 e$  to  $+0.37 e$  and the negative charge on the oxygen increases from  $-0.49 e$  to  $-0.63 e$  (see Table 1). Remarkably, this demonstrates significant medium-range effects of the hydrated calcium cation on the charge of an oxygen centre to which it is bound via a hydrogen bond network (i.e., not covalently bound). The above results indicate that the hydrogen bonding ability of one epoxide group on the GO surface is enhanced by the coordination of the hydrated calcium ion. Such enhancement was shown via the increasing hydrogen bond acceptor strength of GO oxygen and additional hydrogen bonding interactions with the first hydration sphere of calcium cation. It is evident, both theoretically and experimentally, that epoxide groups on a GO surface tend to cluster in islands rather than be uniformly distributed across the surface<sup>26,56</sup>. This leads to a natural question, whether this single hydrated calcium cation can interact with more than one epoxide group on GO surface.

**Table.1** Atomic polar tensor (APT) charge ( $q$ ) in a.u. involved in the hydrogen bonds and on the Ca atom for the systems in Fig. 3.

| Model | $q$ ( $O_{\text{water}}$ ) | $q$ ( $H_{\text{water}}$ ) | $q$ ( $O_{\text{epoxy}}$ ) | $q$ (Ca) |
|-------|----------------------------|----------------------------|----------------------------|----------|
| 3a    | N/A*                       | N/A                        | $-0.40$                    | N/A      |
| 3b    | $-0.49$                    | $+0.27$                    | $-0.47$                    | N/A      |
| 3c    | $-0.48, -0.45$             | $+0.26, +0.23$             | $-0.51$                    | N/A      |
| 3d    | $-0.63$                    | $+0.37$                    | $-0.84$                    | $+1.34$  |
| 3e    | $-0.61, -0.60$             | $+0.40, +0.35$             | $-0.84$                    | $+1.25$  |

\* N/A corresponds to the absence of atomic polar tensor charge.

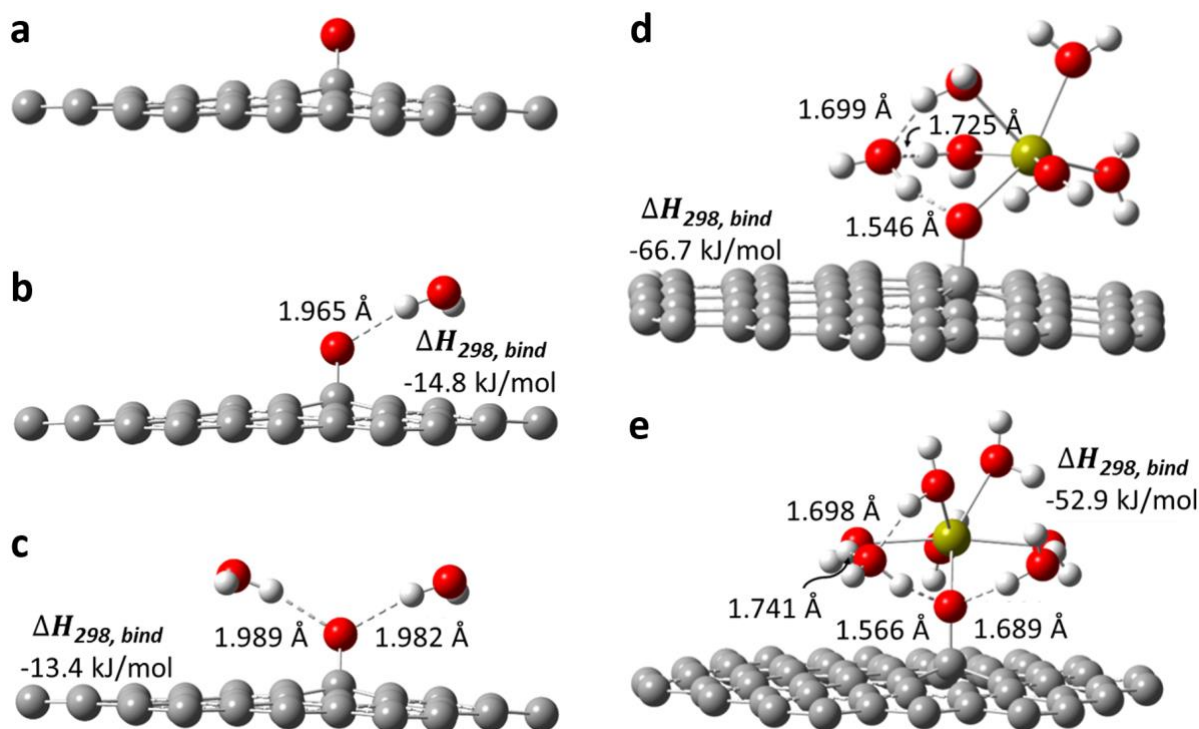


**Fig. 3 Graphene plane-based models for DFT calculations.** **a** Single epoxide group. **b-c** Epoxide group with 1 (**b**) or 2 (**c**) water molecules. **d-e** GO oxygen coordinated to hydrated calcium ion with 1 (**d**) or 2 (**e**) water molecules.  $\Delta H_{298, bind}$  represents hydrogen bond enthalpies. Dashed lines indicate hydrogen bond lengths (selected H-bond distances given in Å).

**Table 2** Comparison between the hydrogen binding enthalpies at 298 K ( $\Delta H_{298, bind}$ , in kJ/mol) for the systems in Fig. 3 obtained in the solid state and in bulk aqueous solution.

| Model | $\Delta H_{298, bind}$ (kJ/mol) |                  |
|-------|---------------------------------|------------------|
|       | Solid state                     | Aqueous solution |
| 3a    | N/A*                            | N/A              |
| 3b    | -14.8                           | -6.8             |
| 3c    | -13.4                           | -5.3             |
| 3d    | -66.7                           | -42.7            |
| 3e    | -52.9                           | -32.9            |

\* N/A corresponds to the absence of hydrogen binding enthalpy.

We further investigate the system with two epoxides on a graphene plane coordinated to a single hydrated calcium ion (see supplementary note 7). Each of the two oxygens on the GO surface is able to hydrogen bond to two water molecules. For the first three water molecules, we obtain binding enthalpies that are similar to those obtained from the functionalized systems in Fig. 3, namely 70.2, 58.5, and 63.6 kJ/mol, respectively. For the fourth water

molecule, we obtain a lower binding enthalpy of 29.9 kJ/mol; this reduction is partly attributed to two (rather than three) hydrogen bonds in which this water molecule is involved in (supplementary note 7). Importantly, all these binding enthalpies are significantly larger than those obtained from the systems with the absence of hydrated calcium cation (Fig. 3b-c).

With the results above, we can now further optimize the hydrogen bond enthalpies from the perspective of the experimental conditions. This is because the calcium-intercalated GO surface in the experimental settings is expected to be intermediate between the solid state and a bulk aqueous solution. It is well-established that hydrogen bond strengths are influenced by the effect of the solvent. In particular, the H-bond strength with the GO surface decreases with the polarity of the medium in the order of solid-state > non-polar solvents > polar solvents. Thus, the calculated hydrogen bond enthalpies above, which do not include solvent corrections, are expected to represent the upper limits for the experimental setting. Therefore, it is instructive to calculate the hydrogen bond enthalpies in bulk aqueous solution to obtain lower limits for the hydrogen-bond enthalpies. For this purpose, we use the conductor-like polarizable continuum model (CPCM)<sup>57</sup>, which has been found to provide good performance for aqueous solution<sup>58,59</sup>. The solvation corrections reduce the hydrogen bond enthalpies for the unfunctionalized GO models by a factor of ~2.5, whereas they reduce the bond enthalpies for the Ca-functionalized GO models by a factor of ~1.5. As shown in Table 2, the inclusion of the solvation corrections widens the gap between the hydrogen bond enthalpies of the GO models with and without coordination of the calcium ion. Considering that the GO surface in the experimental settings is expected to be intermediate between the solid state and a bulk aqueous solution, this is strong evidence to explain our experimental observation.

## Summary

Here, we uncover the synergistic hydrogen-bond network of functionalised carbon in the presence of a hydrated cation. Both our experimental and computational results show a strong increase in hydrogen bond strength in the system of an epoxy functional group in close range to a hydrated calcium ion on a graphene plane. Via AWC experiments we observed that the water uptake per calcium is dramatically increased, by up to a factor of 2.7 times higher in Ca-GOA compared to pure CaCl<sub>2</sub>. Similarly, the water uptake per oxygen of GOA is

dramatically increased by a factor of 8 after intercalation of Ca-ions.

Via extensive DFT calculations, we uncover that the system of hydrated calcium ion and epoxy functional group on graphene plane enhances the overall binding strength of the hydrogen bond network. Particularly, the calcium ion increases the charge polarisation of the oxygen and hydrogen atoms of the C-O bond and water molecules. This leads to a higher enthalpy and shorter hydrogen bond lengths explaining the experimentally observed enhancement of water uptake per calcium ion.

This study holds significance for numerous systems where hydrated ions are in proximity to carbon-based functional groups. As these are omnipresent in nature and technology, our study may help to bring a new perspective to a wide range of natural phenomena and technology applications that involve our described model system. Remarkably, we show that the AWC ability of GO can be enhanced to similar levels as pure CaCl<sub>2</sub> in terms of water uptake per gram. This may open new exciting opportunities to utilise Ca-GOA as a powerful desiccant in atmospheric water generation and energy efficient dehumidification.

## **Methods**

### ***Materials***

The GO solution (15 mg/ml) were prepared via Hummer's method and were supplied by NiSiNa Materials Japan. Calcium chloride (CaCl<sub>2</sub>) dihydrate powder was purchased from Sigma Aldrich.

### ***Synthesis of aerogels***

The Ca-GO solution was prepared by mixing predetermined volume of CaCl<sub>2</sub> salt solution and GO solution, followed by magnetic stirring for 30 mins at 1000 rpm. The as prepared solution was then freeze dried using a vacuum freeze drier at -60 °C to synthesize Ca-GOAs. The GOA samples were prepared by freeze drying the GO solution without further modification. All prepared aerogel samples were stored in vacuum condition until experimental measurements. Synthesized samples are shown in supplementary note 1 (Fig.S1 c-d).

### ***Characterization of aerogels***

The X-ray photoelectron spectrometer (XPS, Thermo Scientific, UK ESCALAB250i) with mono-

chromatic Al K alpha (energy 1486.68 eV) X-ray source was conducted to investigate the chemical composition of the synthesized aerogels. The C1s peak (284.5 eV) of graphite was used as a reference. The surface morphologies of the aerogels were visualized using a field-emission scanning electron microscope (FEI Nova NanoSEM 230 FE-SEM) with an energy dispersive spectroscopy (EDS) detector (Bruker SDD-EDS) for mapping the qualitative elemental composition.

### ***Atmospheric water capture tests***

The atmospheric water capture (AWC) tests of GOAs and Ca-GOAs were carried out in a custom-designed humidity controlling system (see supplementary note 8). The weight changes of the aerogels were continuously recorded every 10 seconds using a computer-controlled mass balance during the AWC process. The humid environment was maintained stable overnight ( $\text{RH} \pm 3\%$ ) before AWC tests. Each experiment was repeated more than 2 times to study the standard deviation.

### ***Computational details***

Density functional theory (DFT) calculations were performed to gain further insights into the experimental findings using the Gaussian 16 software<sup>60</sup>. All geometries were fully optimized using the PBE0 exchange-correlation functional<sup>47</sup> in conjunction with def2-SVP basis set<sup>48</sup> (see supplementary note 9). Empirical dispersion corrections<sup>49</sup> are included using the Becke–Johnson potential (denoted by the suffix D3BJ)<sup>61</sup>. Zero-point vibrational energy and enthalpic temperature corrections have been obtained from these calculations. The equilibrium structures were verified to have all real harmonic frequencies, confirming they are local minima on the potential-energy surface. The final electronic energies were refined using the PBE0-D3BJ functional in conjunction with the much larger quadruple- $\zeta$  def2-QZVPP basis set<sup>48</sup>. Bulk solvent effects in aqueous solution were also considered using the conductor-like polarizable continuum model (CPCM) continuum solvation model<sup>57</sup>.

### **Acknowledgment**

The authors acknowledge the funding for supporting this project from Vesi Water Pty Ltd. X.R. acknowledges the UNSW UIPA Scholarship. The authors acknowledge the staff from Mark Wainwright Analytical Centre at UNSW for technical assistance on sample characterizations

using SEM and XPS. V.Q. acknowledges the funding from the European Union's Horizon 2020 research and innovation programme under the Marie Skłodowska Curie Grant Agreement No. 101066462. The present work was undertaken with the assistance of resources from the National Computational Infrastructure (NCI), which is supported by the Australian Government. We gratefully acknowledge the system administration support provided by the Faculty of Science, Agriculture, Business and Law at the University of New England to the Linux cluster of the Karton group. D.V.A. and K.S.N. are supported by the Ministry of Education, Singapore, under its Research Centre of Excellence award to the Institute for Functional Intelligent Materials (I-FIM, project no. EDUNC-33-18-279-V12). Xiao Sui conducted this work when she was a research scientist in UNSW.

## References

1. Verdaguer, A., Sacha, G. M., Bluhm, H. & Salmeron, M. Molecular Structure of Water at Interfaces: Wetting at the Nanometer Scale. *Chem Rev* **106**, 1478–1510 (2006).
2. Dalin, C., Wada, Y., Kastner, T. & Puma, M. J. Groundwater depletion embedded in international food trade. *Nature* **543**, 700–704 (2017).
3. Björneholm, O. *et al.* Water at Interfaces. *Chem Rev* **116**, 7698–7726 (2016).
4. Barry, E. *et al.* Advanced Materials for Energy-Water Systems: The Central Role of Water/Solid Interfaces in Adsorption, Reactivity, and Transport. *Chem Rev* **121**, 9450–9501 (2021).
5. Yilmaz, G. *et al.* Autonomous atmospheric water seeping MOF matrix. *Sci Adv* **6**, (2020).
6. Hanikel, N. *et al.* Evolution of water structures in metal-organic frameworks for improved atmospheric water harvesting. *Science (1979)* **374**, 454–459 (2021).
7. Yang, Q. *et al.* Capillary condensation under atomic-scale confinement. *Nature* **588**, 250–253 (2020).
8. Tu, Y., Wang, R., Zhang, Y. & Wang, J. Progress and Expectation of Atmospheric Water Harvesting. *Joule* **2**, 1452–1475 (2018).
9. Shan, H. *et al.* Exceptional water production yield enabled by batch-processed portable water harvester in semi-arid climate. *Nat Commun* **13**, 5406 (2022).
10. Lu, H. *et al.* Materials Engineering for Atmospheric Water Harvesting: Progress and Perspectives. *Advanced Materials* **34**, (2022).
11. Levental, I. & Lyman, E. Regulation of membrane protein structure and function by their lipid nano-environment. *Nat Rev Mol Cell Biol* **24**, 107–122 (2023).
12. Harayama, T. & Riezman, H. Understanding the diversity of membrane lipid



- composition. *Nat Rev Mol Cell Biol* **19**, 281–296 (2018).
13. Zhu, Y. *et al.* Regulation of molecular transport in polymer membranes with voltage-controlled pore size at the angstrom scale. *Nat Commun* **14**, 2373 (2023).
  14. Stuart, M. A. C. *et al.* Emerging applications of stimuli-responsive polymer materials. *Nat Mater* **9**, 101–113 (2010).
  15. Foller, T. *et al.* Mass Transport via In-Plane Nanopores in Graphene Oxide Membranes. *Nano Lett* **22**, 4941–4948 (2022).
  16. Wen, X. *et al.* Understanding water transport through graphene-based nanochannels via experimental control of slip length. *Nat Commun* **13**, 5690 (2022).
  17. Joshi, R. K. *et al.* Precise and ultrafast molecular sieving through graphene oxide membranes. *Science (1979)* **343**, 752–754 (2014).
  18. Hung, W.-S. *et al.* Tuneable interlayer spacing self-assembling on graphene oxide-framework membrane for enhance air dehumidification. *Sep Purif Technol* **239**, 116499 (2020).
  19. Ren, X. *et al.* Graphene oxide membranes for effective removal of humic acid. *J Mater Res* **37**, 3362–3371 (2022).
  20. Xia, C. *et al.* General synthesis of single-atom catalysts with high metal loading using graphene quantum dots. *Nat Chem* **13**, 887–894 (2021).
  21. Qiao, B. *et al.* Single-atom catalysis of CO oxidation using Pt<sub>1</sub>/FeO<sub>x</sub>. *Nat Chem* **3**, 634–641 (2011).
  22. Dreyer, D. R., Park, S., Bielawski, C. W. & Ruoff, R. S. The chemistry of graphene oxide. *Chem. Soc. Rev.* **39**, 228–240 (2010).
  23. Chen, D., Feng, H. & Li, J. Graphene Oxide: Preparation, Functionalization, and Electrochemical Applications. *Chem Rev* **112**, 6027–6053 (2012).
  24. Khine, Y. Y. *et al.* Surface Functionalities of Graphene Oxide with Varying Flake Size. *Ind Eng Chem Res* **61**, 6531–6536 (2022).
  25. Yan, J.-A., Xian, L. & Chou, M. Y. Structural and Electronic Properties of Oxidized Graphene. *Phys Rev Lett* **103**, 086802 (2009).
  26. Foller, T. *et al.* Enhanced graphitic domains of unreduced graphene oxide and the interplay of hydration behaviour and catalytic activity. *Materials Today* **50**, 44–54 (2021).
  27. Abraham, J. *et al.* Tunable sieving of ions using graphene oxide membranes. *Nature Nanotechnology* 2017 12:6 **12**, 546–550 (2017).
  28. Zhang, S. *et al.* Ultrathin Membranes for Separations: A New Era Driven by Advanced Nanotechnology. *Advanced Materials* **34**, 2108457 (2022).

29. Kumar, P. V. *et al.* Scalable enhancement of graphene oxide properties by thermally driven phase transformation. *Nature Chemistry* 2013 6:2 **6**, 151–158 (2013).
30. Sun, P. *et al.* Selective ion penetration of graphene oxide membranes. *ACS Nano* **7**, 428–437 (2013).
31. Nie, L. *et al.* Realizing small-flake graphene oxide membranes for ultrafast size-dependent organic solvent nanofiltration. *Sci Adv* **6**, (2020).
32. Lerf, A. *et al.* Hydration behavior and dynamics of water molecules in graphite oxide. *Journal of Physics and Chemistry of Solids* **67**, 1106–1110 (2006).
33. Mouhat, F., Coudert, F.-X. & Bocquet, M.-L. Structure and chemistry of graphene oxide in liquid water from first principles. *Nat Commun* **11**, 1566 (2020).
34. Wang, F., You, Y., Jin, X. & Joshi, R. On the role of driving force in water transport through nanochannels within graphene oxide laminates. *Nanoscale* **10**, 21625–21628 (2018).
35. Zhang, X. J. & Qiu, L. M. Moisture transport and adsorption on silica gel–calcium chloride composite adsorbents. *Energy Convers Manag* **48**, 320–326 (2007).
36. Long, Y. *et al.* Molecule Channels Directed by Cation-Decorated Graphene Oxide Nanosheets and Their Application as Membrane Reactors. *Advanced Materials* **29**, (2017).
37. Lian, B. *et al.* Extraordinary water adsorption characteristics of graphene oxide. *Chem Sci* **9**, 5106–5111 (2018).
38. Zhang, X. J., Sumathy, K., Dai, Y. J. & Wang, R. Z. Parametric study on the silica gel–calcium chloride composite desiccant rotary wheel employing fractal BET adsorption isotherm. *Int J Energy Res* **29**, 37–51 (2005).
39. Brunauer, S., Emmett, P. H. & Teller, E. Adsorption of Gases in Multimolecular Layers. *J Am Chem Soc* **60**, 309–319 (1938).
40. Fripiat, J. J., Gatinéau, L. & Van Damme, H. Multilayer physical adsorption on fractal surfaces. *Langmuir* **2**, 562–567 (1986).
41. Freundlich, H. Über die Adsorption in Lösungen. *Zeitschrift für Physikalische Chemie* **57U**, 385–470 (1907).
42. Foo, K. Y. & Hameed, B. H. Insights into the modeling of adsorption isotherm systems. *Chemical Engineering Journal* **156**, 2–10 (2010).
43. Swenson, H. & Stadie, N. P. Langmuir’s Theory of Adsorption: A Centennial Review. *Langmuir* **35**, 5409–5426 (2019).
44. Freundlich, H. Über die Adsorption in Lösungen. *Zeitschrift für Physikalische Chemie* **57U**, 385–470 (1907).
45. Kalam, S., Abu-Khamsin, S. A., Kamal, M. S. & Patil, S. Surfactant Adsorption Isotherms:

- A Review. *ACS Omega* **6**, 32342–32348 (2021).
46. Buchsteiner, A., Lerf, A. & Pieper, J. Water Dynamics in Graphite Oxide Investigated with Neutron Scattering. *J Phys Chem B* **110**, 22328–22338 (2006).
  47. Perdew, J. P., Burke, K. & Ernzerhof, M. Generalized Gradient Approximation Made Simple. *Phys Rev Lett* **77**, 3865–3868 (1996).
  48. Weigend, F. & Ahlrichs, R. Balanced basis sets of split valence, triple zeta valence and quadruple zeta valence quality for H to Rn: Design and assessment of accuracy. *Physical Chemistry Chemical Physics* **7**, 3297 (2005).
  49. Grimme, S., Antony, J., Ehrlich, S. & Krieg, H. A consistent and accurate *ab initio* parametrization of density functional dispersion correction (DFT-D) for the 94 elements H-Pu. *J Chem Phys* **132**, (2010).
  50. Steiner, T. The Hydrogen Bond in the Solid State. *Angewandte Chemie International Edition* **41**, 48–76 (2002).
  51. Sigala, P. A. *et al.* Determination of Hydrogen Bond Structure in Water versus Aprotic Environments To Test the Relationship Between Length and Stability. *J Am Chem Soc* **137**, 5730–5740 (2015).
  52. Weinhold, F. & Klein, R. A. What is a hydrogen bond? Mutually consistent theoretical and experimental criteria for characterizing H-bonding interactions. *Mol Phys* **110**, 565–579 (2012).
  53. Saito, A., Obata, S. & Nishina, Y. Uniform coating of magnesium oxide crystal with reduced graphene oxide achieves moisture barrier performance. *Appl Surf Sci* **573**, 151483 (2022).
  54. Cioslowski, J. A new population analysis based on atomic polar tensors. *J Am Chem Soc* **111**, 8333–8336 (1989).
  55. De Proft, F., Martin, J. M. L. & Geerlings, P. On the performance of density functional methods for describing atomic populations, dipole moments and infrared intensities. *Chem Phys Lett* **250**, 393–401 (1996).
  56. Shin, D. S. *et al.* Distribution of oxygen functional groups of graphene oxide obtained from low-temperature atomic layer deposition of titanium oxide. *RSC Adv* **7**, 13979–13984 (2017).
  57. Cossi, M., Rega, N., Scalmani, G. & Barone, V. Energies, structures, and electronic properties of molecules in solution with the C-PCM solvation model. *J Comput Chem* **24**, 669–681 (2003).
  58. Takano, Y. & Houk, K. N. Benchmarking the Conductor-like Polarizable Continuum Model (CPCM) for Aqueous Solvation Free Energies of Neutral and Ionic Organic Molecules. *J Chem Theory Comput* **1**, 70–77 (2005).
  59. Skyner, R. E., McDonagh, J. L., Groom, C. R., van Mourik, T. & Mitchell, J. B. O. A review

of methods for the calculation of solution free energies and the modelling of systems in solution. *Physical Chemistry Chemical Physics* **17**, 6174–6191 (2015).

60. Frisch, M. J. *et al.* Gaussian 16, Revision C.01. Preprint at (2016).
61. Grimme, S., Ehrlich, S. & Goerigk, L. Effect of the damping function in dispersion corrected density functional theory. *J Comput Chem* **32**, 1456–1465 (2011).